Supporting Information

Rapid and long-lasting acceleration of zero-valent iron nanoparticles@Ti_3C_2-based MXene/peroxymonosulfate oxidation with bi-active centers toward ranitidine removal

Yiyang Ma[1,2,3], Dongbin Xiong[4], Xiaofan Lv[5], Xuesong Zhao[1,2,3], Chenchen Meng[1,2,6], Haijiao Xie[7], and Zhenghua Zhang[1,2,3*]

[1] Institute of Environmental Engineering & Nano-Technology, Tsinghua Shenzhen International Graduate School, Tsinghua University, Shenzhen 518055, Guangdong, China

[2] Guangdong Provincial Engineering Research Center for Urban Water Recycling and Environmental Safety, Tsinghua Shenzhen International Graduate School, Tsinghua University, Shenzhen 518055, Guangdong, China

[3] School of Environment, Tsinghua University, Beijing 100084, China

[4] Pillar of Engineering Product Development, Singapore University of Technology and Design, Singapore 487372, Singapore

[5] Beijing Key Laboratory of Water Resources & Environmental Engineering, China University of Geosciences (Beijing), Beijing 100083, China

[6] College of Chemistry and Environmental Engineering, Shenzhen University, Shenzhen 518060, China

[7] Hangzhou Yanqu Information Technology Co., Ltd., Hangzhou 310003, China

Journal of Materials Chemistry A

Revised version

Submitted April, 2021

*Corresponding author: E-mail: zhenghua.zhang@sz.tsinghua.edu.cn (Z. Zhang).

Text S1. Chemicals and reagents used in this study

Ferrous sulfate ($FeSO_4$, >98.0%, AR, Macklin), Sodium borohydride ($NaBH_4$, 98.0%, AR, Innochem), Lithium fluoride (LiF, 99.9%, AR, Aladdin), Hydrochloric acid (HCl, 36.0%wt, Guangzhou Chemical Reagent Factory), Sodium hydroxide (NaOH, 96.0%, AR, Macklin), Sodium chloride (NaCl, 99.9%, AR, Macklin), Sodium bicaronate ($NaHCO_3$, 99.8%, AR, Macklin), Sodium sulfate (Na_2SO_4, 99%, AR, Macklin), Sodium nitrate ($NaNO_3$, 99.0%, AR, Aladdin), Postassium peroxymonosulfate (PMS, 98.0%wt, Ann nike), tert-butyl alcohol (TBA, >99.0%, AR, Macklin), anhydrous ethanol (EtOH, >99.7%, AR, Ann nike), Ranitidine (>98.0%, Tokyo Huacheng Industry), 5,5-dimethyl-pyrroline-N-oxide (DMPO, 97.0%, AR, Macklin) and Sodium thiosulfate ($NaS_2O_3 \cdot 5H_2O$, 99.0%, AR, Macklin). Milli-Q water deionized using Aquelix 5 (Millipore, America) is used as the solvent.

Text S2. Density functional theory (DFT) calculations

We have employed the Vienna Ab Initio Package (VASP)[1,2] to perform all the density functional theory (DFT) calculations within the generalized gradient approximation (GGA) using the PBE formulation[3]. We have chosen the projected augmented wave (PAW) potentials[4,5] to describe the ionic cores and take valence electrons into account using a plane wave basis set with a kinetic energy cutoff of 400 eV. Partial occupancies of the Kohn−Sham orbitals were allowed using the Gaussian smearing method and a width of 0.05 eV. The electronic energy was considered self-consistent when the energy change was smaller than 10^{-5} eV. A geometry optimization was considered convergent when the force change was smaller than 0.02 eV/Å. Grimme's DFT-D3 methodology[6] was used to describe the dispersion interactions.

The equilibrium lattice constant of hexagonal $Ti_3C_2T_x(001)$ unit cell with a vaccum layer in the depth of 15 Å was optimized, when using a 13×13×1 Monkhorst-Pack k-point grid for Brillouin zone sampling, to be a=3.162 Å. We then use it to construct a $Ti_3C_2T_x(001)$ supercell model with p(4×4) periodicity in the x and y directions. This surface model contains 48 Ti, 32 C, 32 O and 32 H atoms. In another model, a Fe_4 metal cluster resides on top the $Ti_3C_2T_x(001)$ supercell model. During structural optimizations for both surface models, the gamma point in the Brillouin zone was used for k-point sampling, and all atoms were allowed to relax.

The adsorption energy (E_{ads}) of adsorbate A was defined as: $\boldsymbol{E_{ads} = E_{A/surf} - E_{surf} - E_{A(g)}}$

where $E_{A/surf}$, E_{surf} and $E_{A(g)}$ are the energy of adsorbate A adsorbed on the surface, the energy of clean surface, and the energy of isolated A molecule in a cubic periodic box with a side length of 20 Å and a 1×1×1 Monkhorst-Pack k-point grid for Brillouin zone sampling, respectively.

Finally, transition states for elementary reaction steps were determined by a combination of the nudged elastic band (NEB) method[7] and the dimer method[8-10]. In the NEB method, the path between the reactant and product is discretized into a series of structural images. The image that is closest to a likely transition state structure was then employed as an initial guess structure for the dimer method.

Text S3. The method of electro-chemical measurement

The nZVIPs and nZVIPs@Ti_3C_2 nanosheets electrodes were prepared by mixing with active composite (70 wt%), carbon black (20 wt%), and polyvinylidene fluoride (10 wt%) in N-methyl-2-pyrrolidone solvent. The mixture slurry was cast onto a copper foil as the current collector, and then vacuum dried at 80℃ for 12 h. The average mass loading of each electrode was about 1.0 $mg \cdot cm^{-2}$, with a diameter of 12 mm. The CR2032 coin-type cell was assembled with the as-prepared electrodes (nZVIPs and nZVIPs@Ti_3C_2 nanosheets), encounter electrode (lithium foil), separator (polypropylene, Celgard 2400), and electrolyte (1 M $LiPF_6$ in DOL/DME (v/v=1:1) with 0.1 M $LiNO_3$ additives). Electrochemical impedance spectroscopy (EIS) measurements were conducted on an AUTOLAB eletrochemical workstation in the frequency range of 100 kHz - 10 mHz with an amplitude of 5 mV.

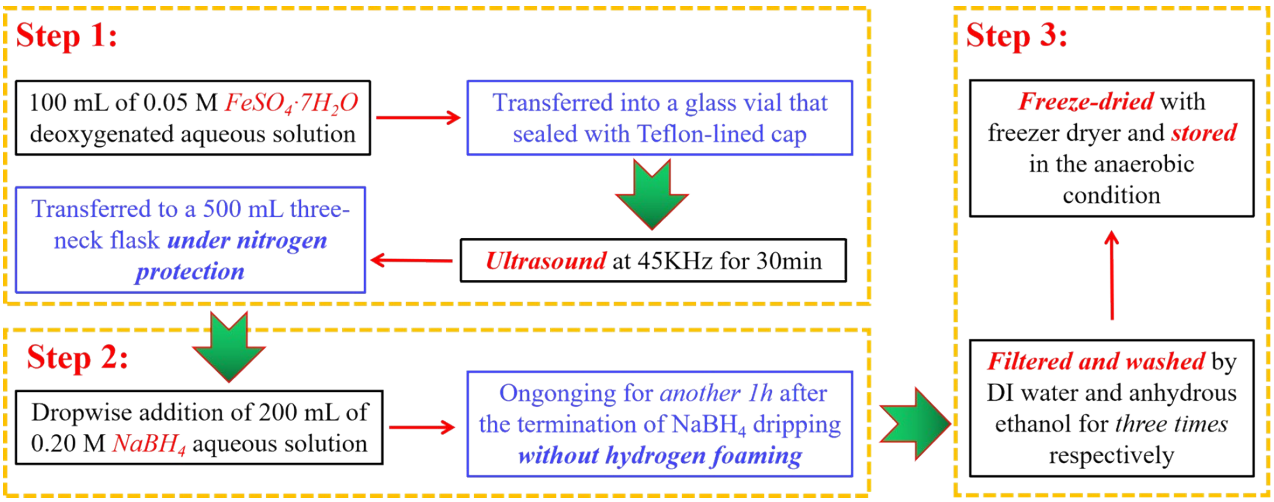

Fig. S1. Schematic diagram of nanoscale zero-valent iron particles preparation.

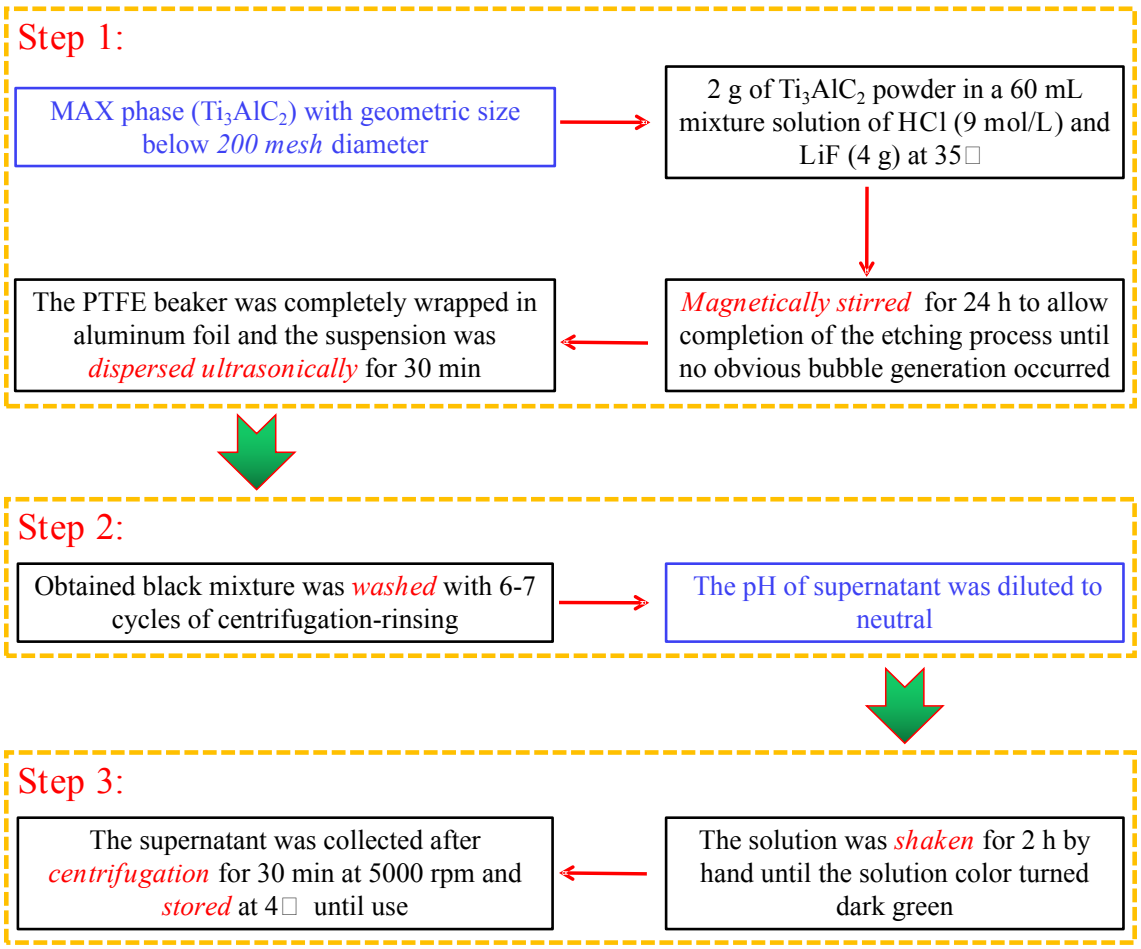

Fig. S2. Schematic diagram of Ti_3C_2-based MXene preparation.

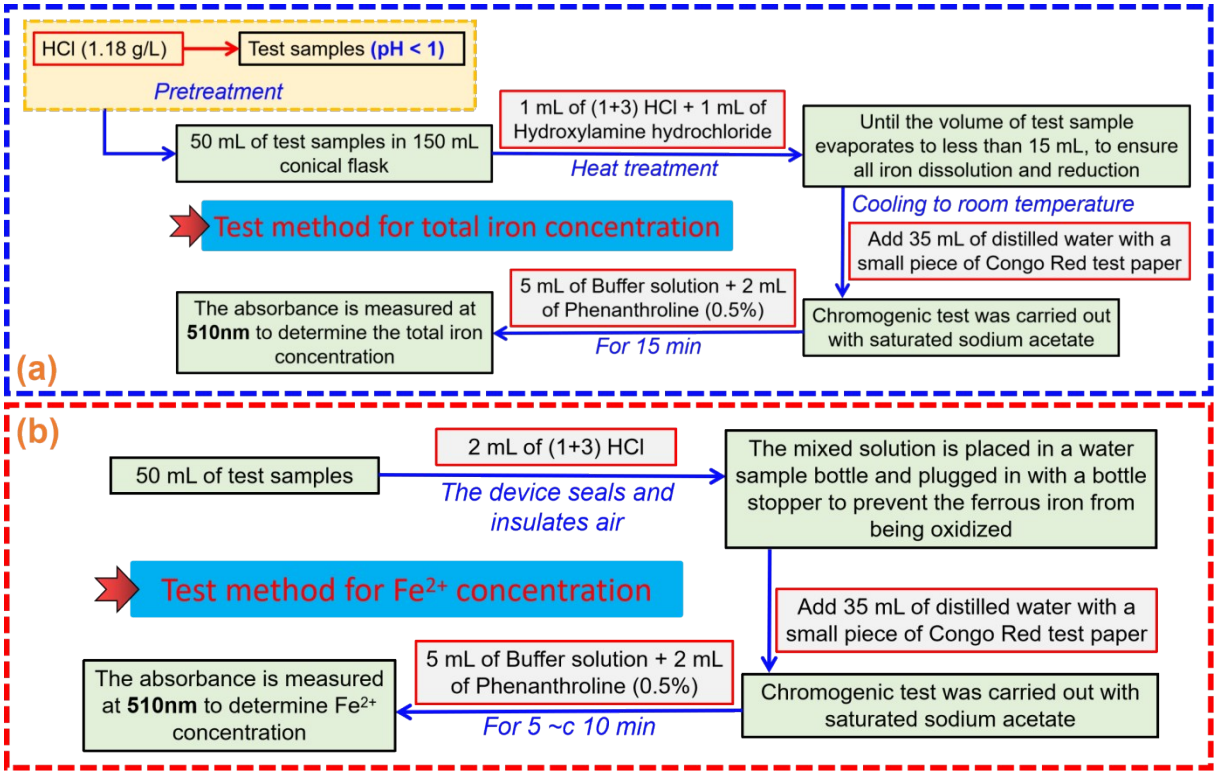

Fig. S3. The procedures of the Water quality-Determination of Iron-phenanthroline spectrophotometry.

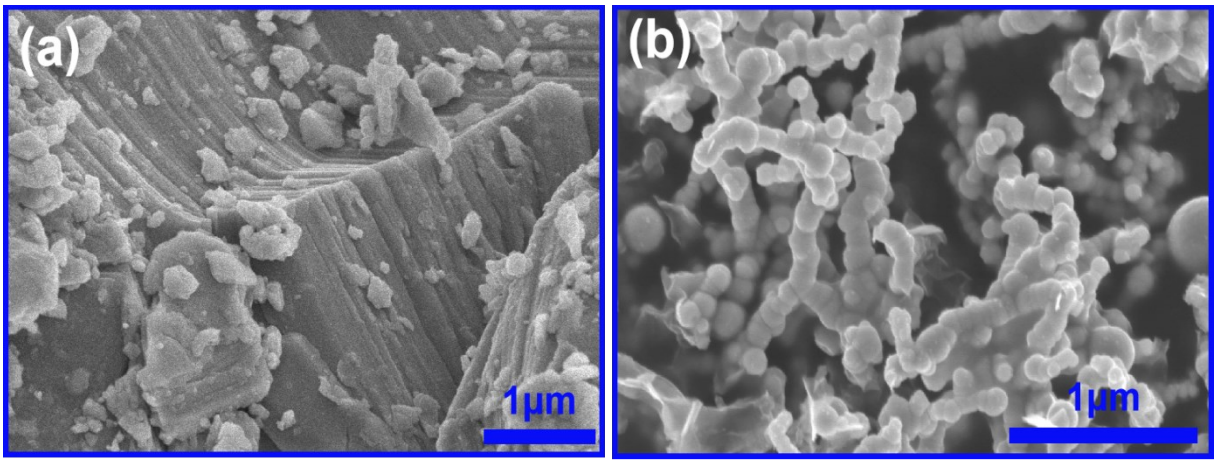

Fig. S4. SEM images of (a) Ti_3AlC_2 MAX phase and (b) nanoscale zero-valent iron particles (nZVIPs).

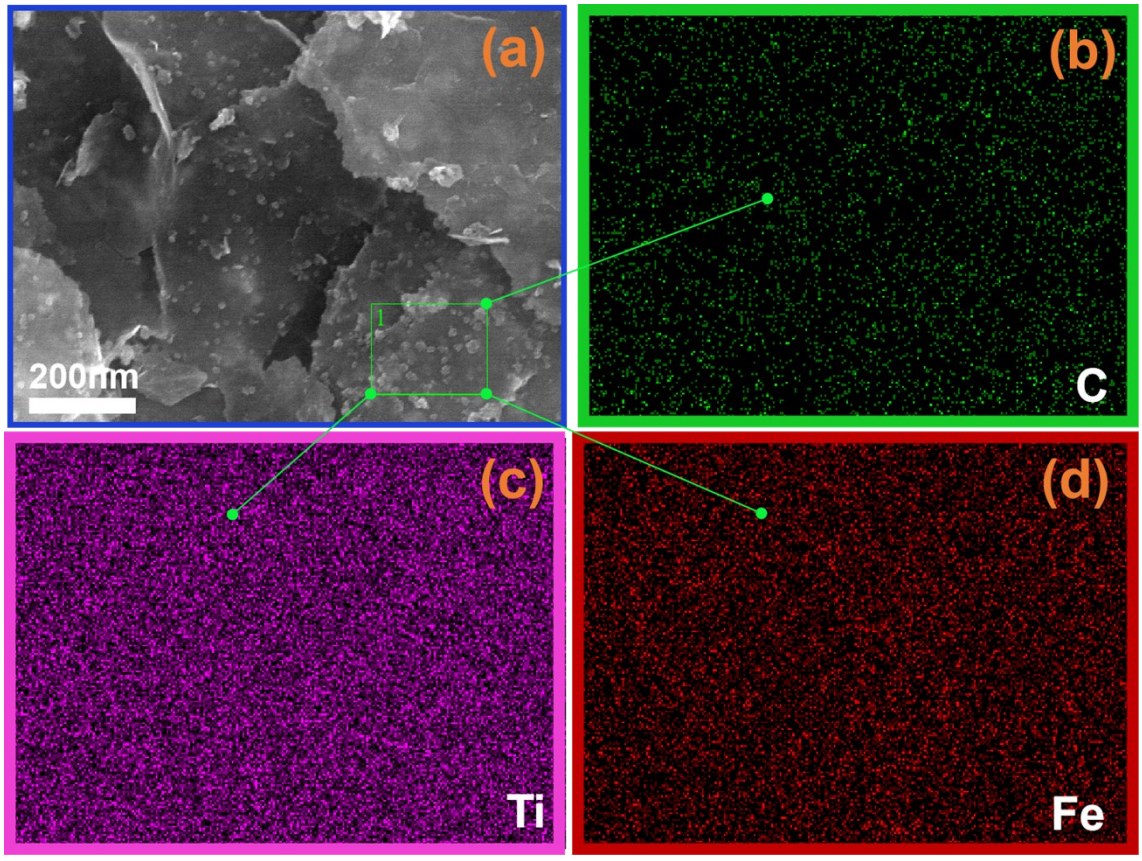

Fig. S5. SEM image of nZVIPs@Ti_3C_2 nanosheets ***(a)*** and the corresponding elemental mapping of ***(b)*** carbon, ***(c)*** titanium and ***(d)*** iron.

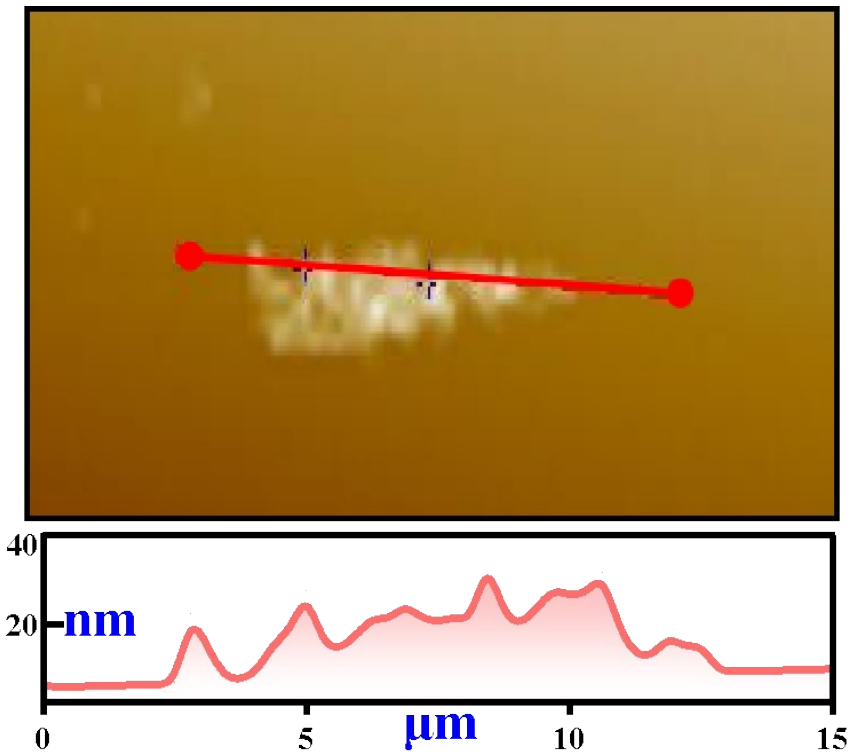

Fig. S6. AFM image of nZVIPs@Ti_3C_2 nanosheets.

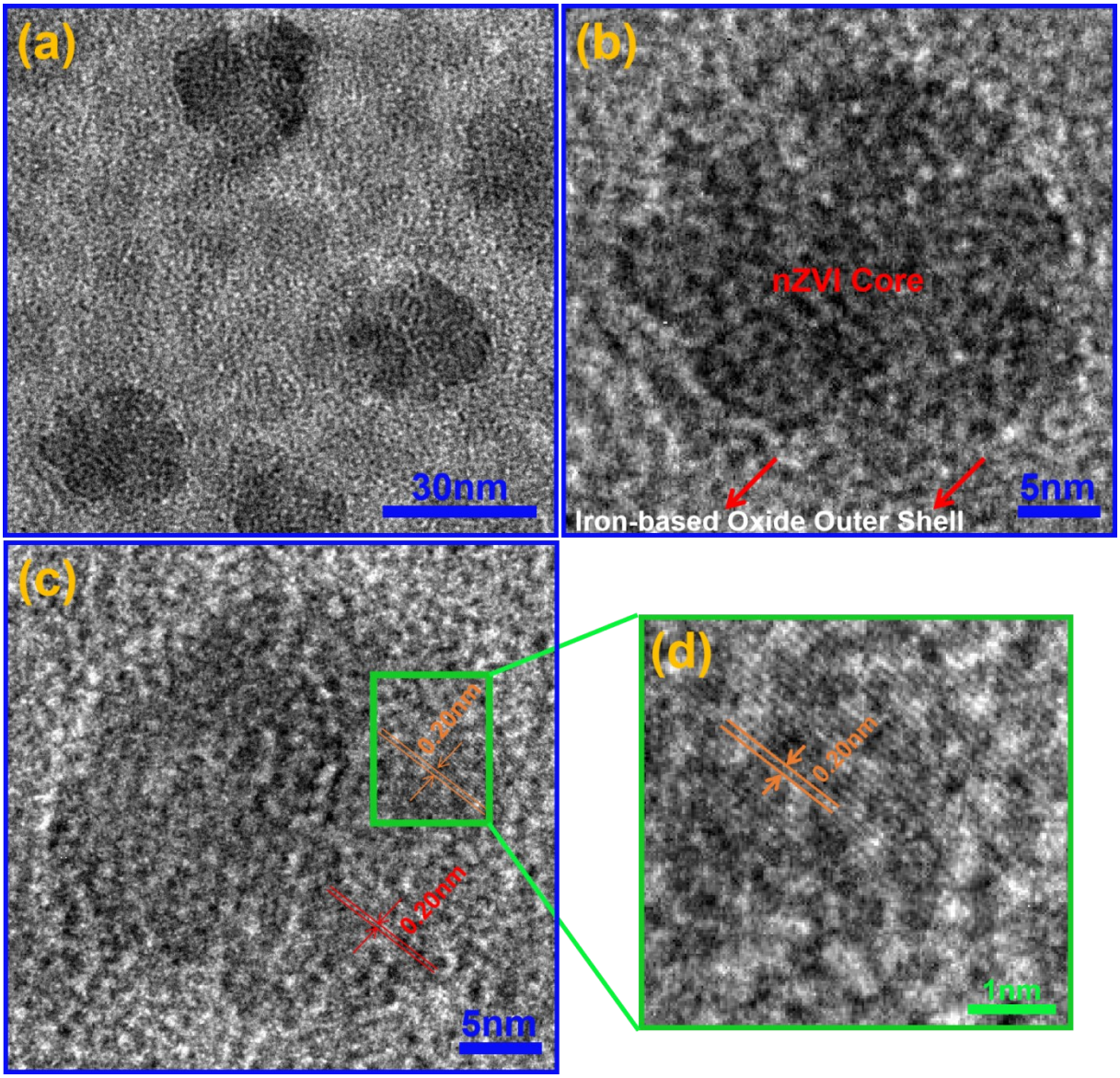

Fig. S7. The HRTEM images of nZVIPs@Ti_3C_2 nanosheets at different magnification scales (30 nm, 5 nm and 1 nm).

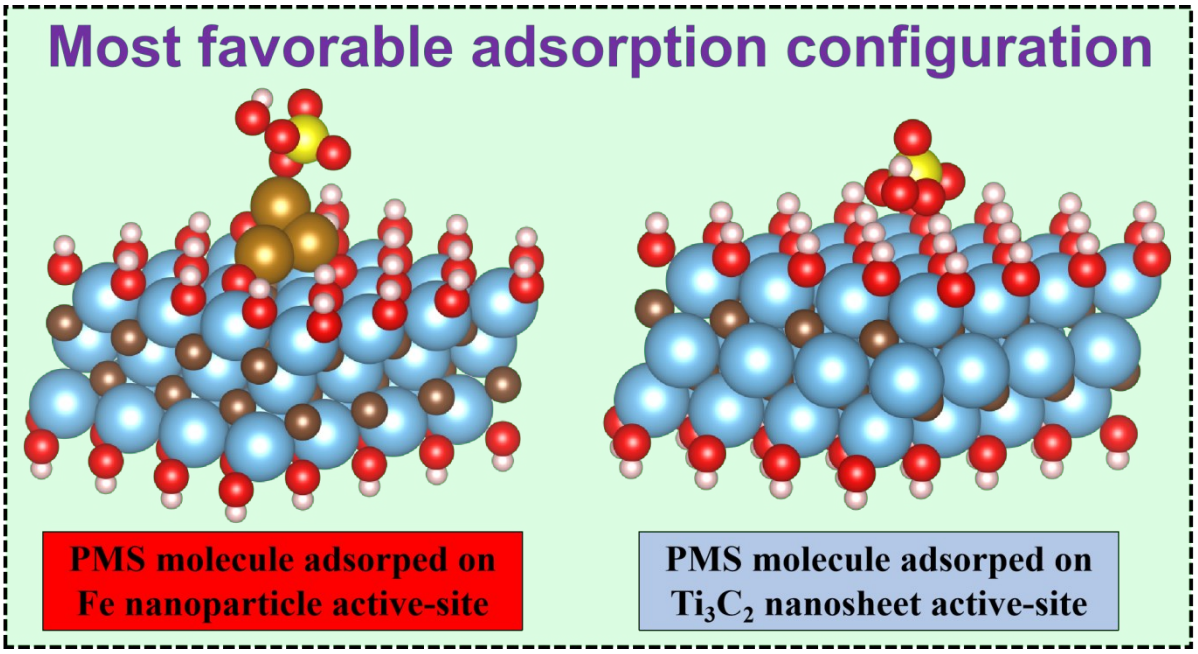

Fig. S8. The most favorable adsorption configurations of PMS molecule on nZVPs@Ti_3C_2 and Ti_3C_2 nanosheets.

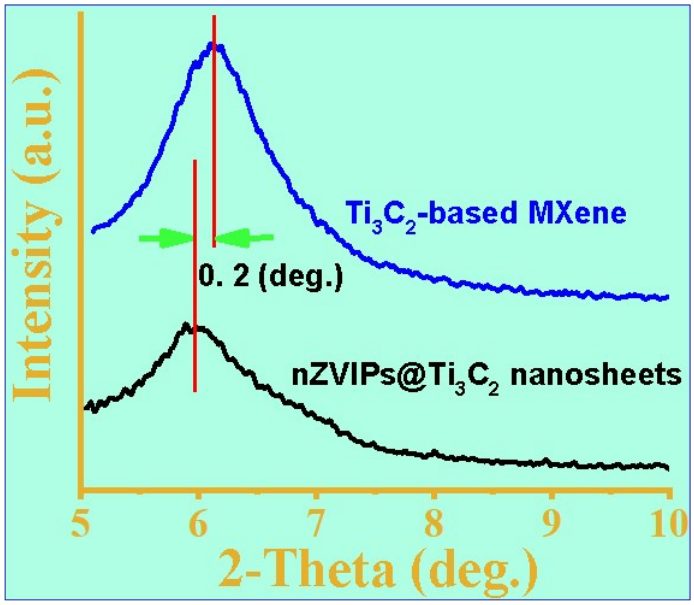

Fig. S9. XRD patterns of Ti_3C_2-based MXene and nZVIPs@Ti_3C_2 nanosheets.

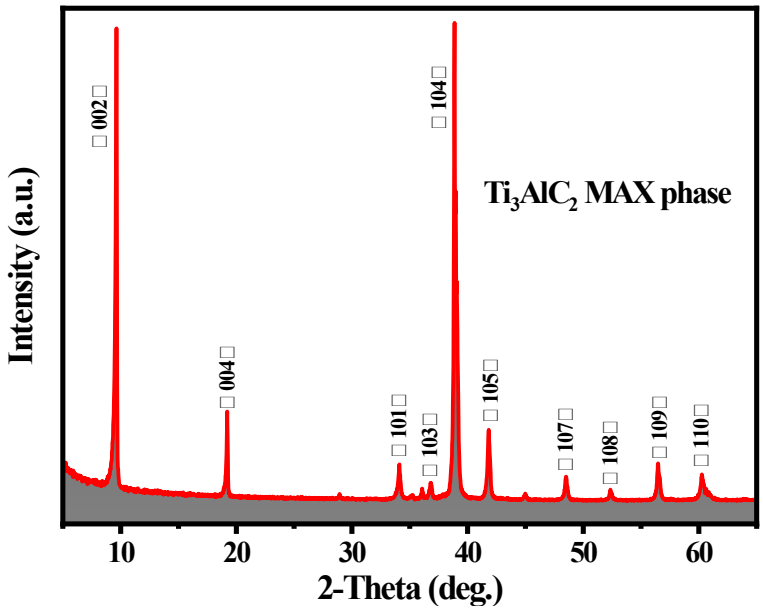

Fig. S10. XRD pattern of Ti_3AlC_2 MAX phase.

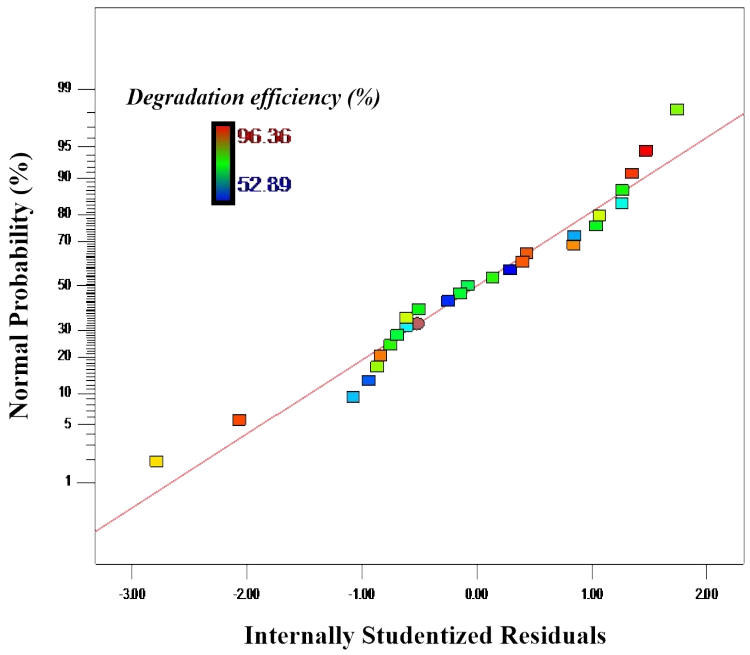

Fig. S11. Probability relationship between internally standardized residuals and normal probability.

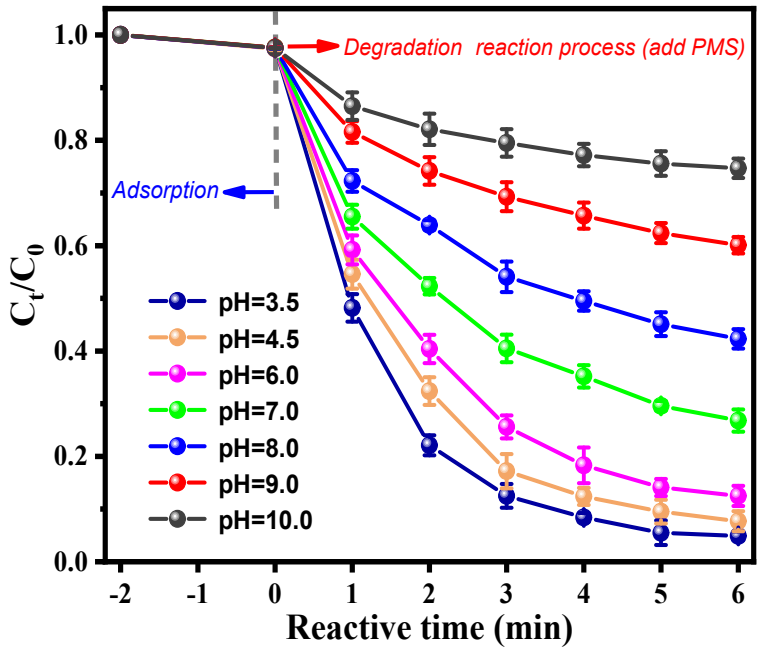

Fig.S12. Effect of initial solution pH on degradation of ranitidine in the nZVIPs@Ti_3C_2 nanosheets/PMS system. Experimental conditions: $[Ranitidine]_0$ = 10 mg/L, $[PMS]_0$ = 0.1 g/L, $[Cata]_0$ = 75 mg/L, nZVI/Ti_3C_2 mass ratio = 1:1, at room temperature.

As illustrated in ***Fig.S12***, the catalytic activity of nZVIPs@Ti_3C_2 nanosheets for ranitidine removal was observed to be highly pH-dependent and the corresponding removal efficiency reached 95.12 ± 0.85%, 92.34 ± 0.19%, 87.53 ± 0.19%, 73.24 ± 0.21%, 57.75 ± 0.18%, 39.92 ± 0.16% and 25.34 ± 0.18% after 6 min, when the initial solution pH value was adjusted to 3.5, 4.5, 6.0, 7.0, 8.0, 9.0 and 10.0, respectively. Overall, under neutral and basic conditions, the dominant radical species exhibited weaken oxidation capability and shorter life span, resulting in the decline of removal efficiency toward ranitidine.

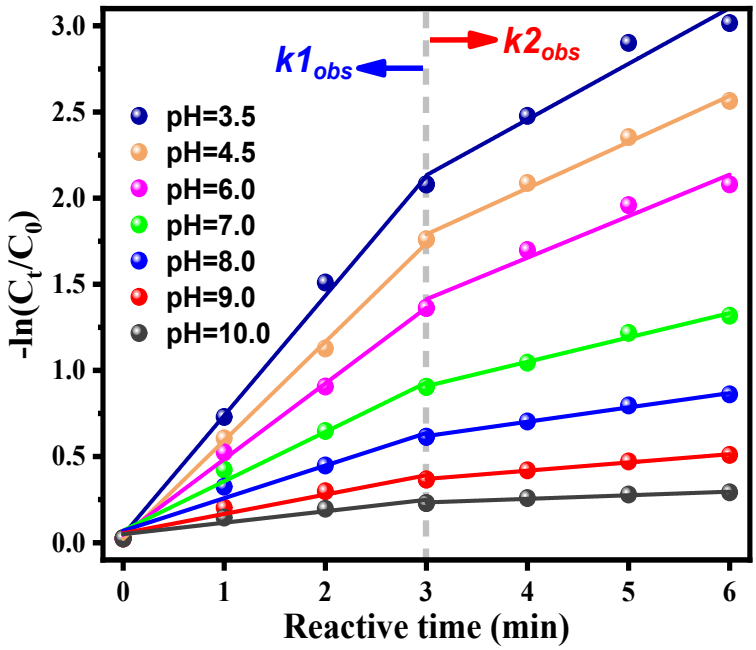

Fig.S13. Effect of initial solution pH on the reaction rate constant of ranitidine removal. Experimental conditions: $[Ranitidine]_0$ = 10 mg/L, $[PMS]_0$ = 0.1 g/L, $[Cata]_0$ = 75 mg/L, nZVI/Ti_3C_2 mass ratio = 1:1, at room temperature.

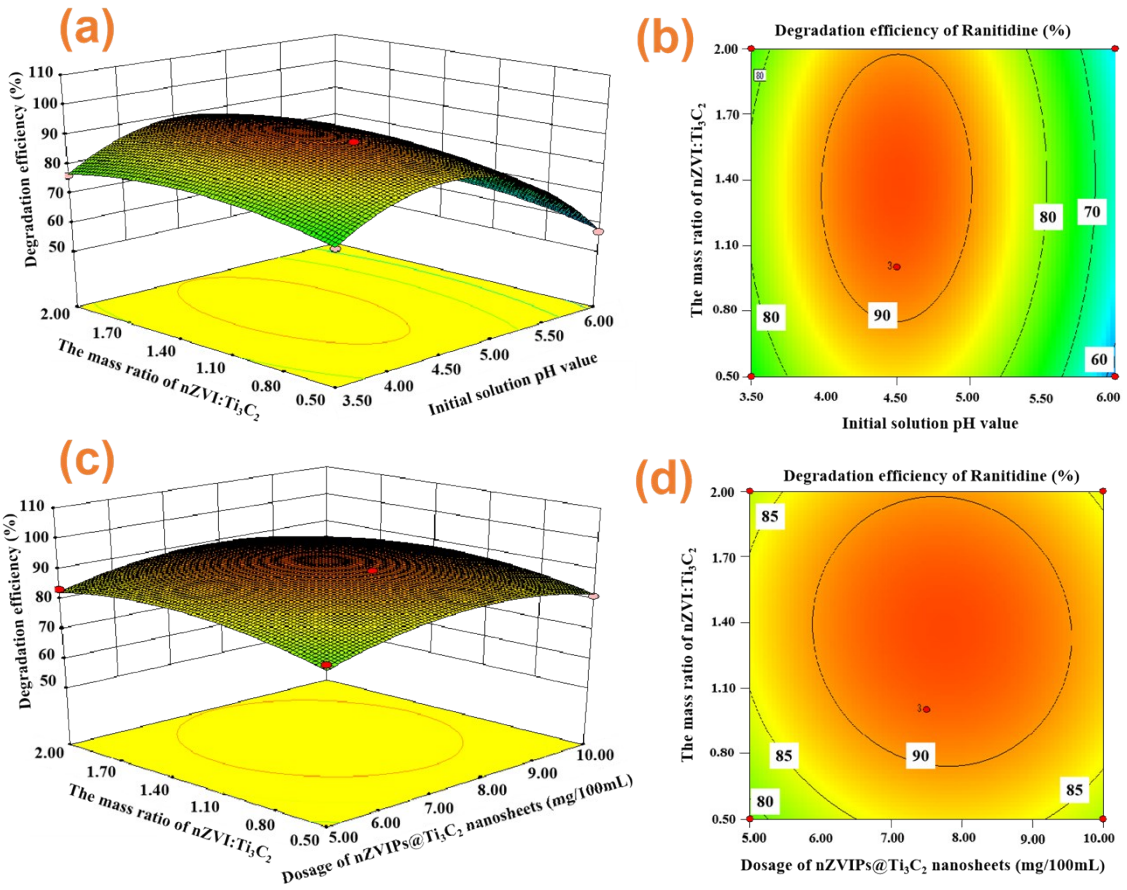

Fig.S14. Three-dimensional and contour maps of interaction between different factors for ranitidine degradation efficiency, (a) and (b) initial solution pH value and the mass ratio of nZVI:Ti_3C_2; (c) and (d) dosage of nZVIPs@Ti_3C_2 nanosheets and the mass ratio of nZVI:Ti_3C_2.

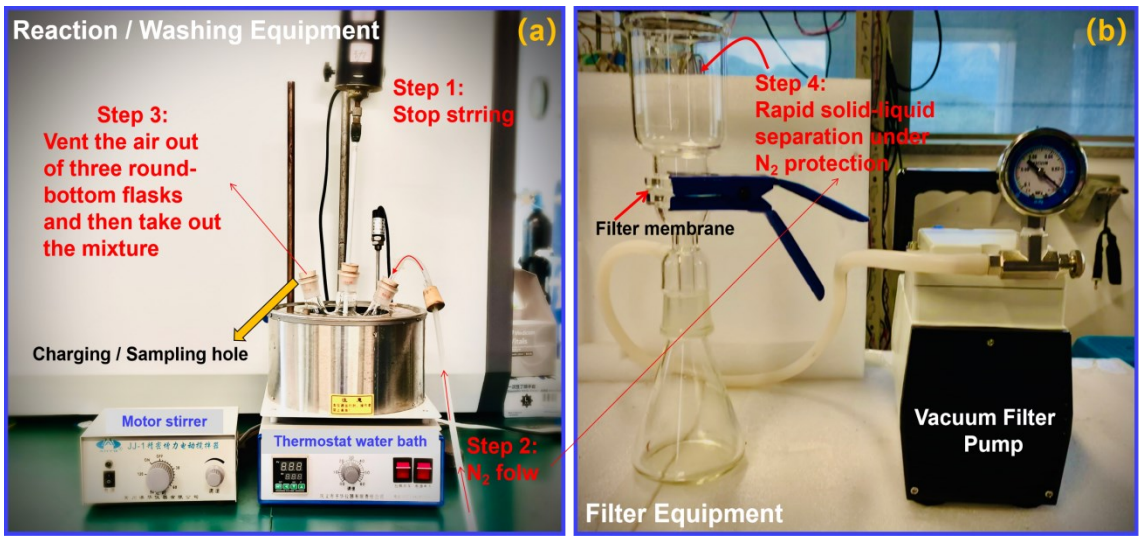

Fig. S15. The pretreatment process of nZVIPs@Ti_3C_2 nanosheets before the next experimental cycle.

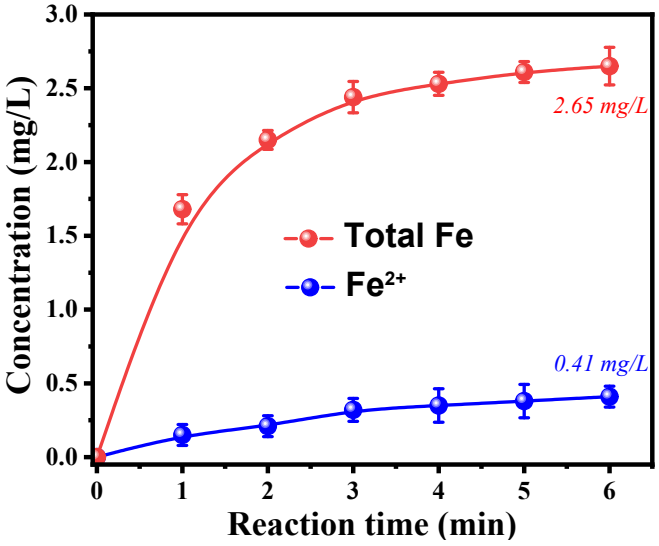

Fig. S16. Concentrations of total iron and ferrous ions in solution during the catalytic process in nZVIPs@Ti_3C_2 nanosheets/PMS system. Experimental conditions: $[Ranitidine]_0$ = 10 mg/L, $[PMS]_0$ = 0.1 g/L, $[Cata]_0$ = 75 mg/L, nZVI/Ti_3C_2 mass ratio = 1:1, the initial solution pH = 4.5, at room temperature.

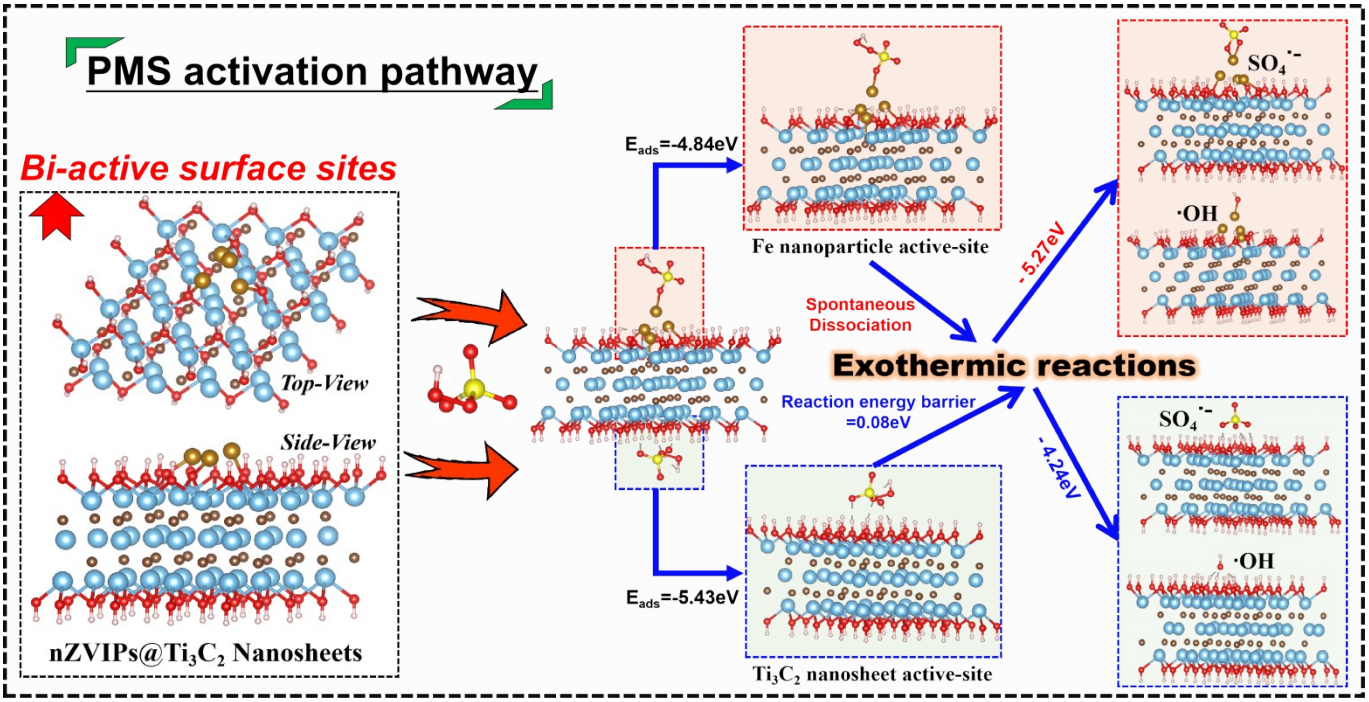

Fig. S17. The activation pathway of PMS molecules on the bi-active surface sites of nZVIPs@Ti_3C_2 nanosheets. Blue, brown, gold, yellow, red, and white balls represent Ti, C, Fe, S, O, and H atoms, respectively.

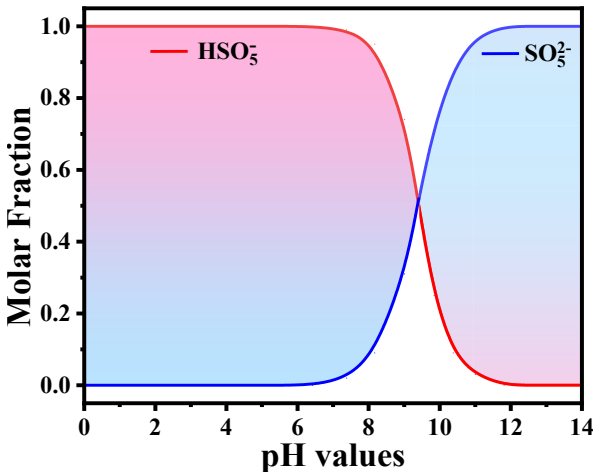

Fig. S18. PMS species under different pH conditions.

Table S1. The atomic and weight ratios of each element in nZVIPs@Ti_3C_2 nanosheets.

Element	Weight (%)	Atomic (%)	Uncert. (%)	Correction
O	*38.47*	*61.38*	*1.28*	*0.51*
Ti	*10.73*	*4.89*	*0.57*	*0.98*
Fe	*22.64*	*11.26*	*0.63*	*0.99*
C	*28.14*	*19.46*	*0.86*	*0.99*

Table S2. Physicochemical properties of nZVIPs, Ti_3C_2-based MXene and nZVIPs@Ti_3C_2 nanosheets.

Sample	Particle size (nm)	S_{BET} (m^2/g)	Pore size (nm)	Pore volume (cm^2/g)
nZVIPs	*100-250*	*14.56*	*28.19*	*0.11*
Ti_3C_2-based MXene	--	*107.82*	*11.58*	*0.31*
nZVIPs@Ti_3C_2 nanosheets	*10-30*	*28.25*	*36.44*	*0.26*

Table S3. Experimental design and results.

Test serial number	X_1	X_2 (mg/100mL)	X_3 (mg/100mL)	X_4	Actual values R_1 (%)	Predicted values R_2 (%)
1	*3.5*	*5*	*7.5*	*1:1*	*63.62*	*64.22*
2	*6.0*	*5*	*7.5*	*1:1*	*52.89*	*52.62*
3	*3.5*	*20*	*7.5*	*1:1*	*90.35*	*89.64*
4	*6.0*	*20*	*7.5*	*1:1*	*64.81*	*64.00*
5	*4.5*	*10*	*7.5*	*1:1*	*91.28*	*92.18*
6	*4.5*	*10*	*10*	*1:2*	*81.25*	*82.07*
7	*4.5*	*10*	*5*	*2:1*	*83.52*	*82.73*
8	*4.5*	*10*	*10*	*2:1*	*83.56*	*84.01*
9	*3.5*	*10*	*7.5*	*1:2*	*74.15*	*74.65*
10	*6.0*	*10*	*7.5*	*1:2*	*56.89*	*57.75*
11	*3.5*	*10*	*7.5*	*2:1*	*76.32*	*76.95*
12	*6.0*	*10*	*7.5*	*2:1*	*61.22*	*61.90*
13	*4.5*	*5*	*5*	*1:1*	*71.39*	*71.46*
14	*4.5*	*10*	*7.5*	*1:1*	*92.65*	*92.18*
15	*4.5*	*10*	*5*	*1:1*	*73.57*	*72.58*
16	*4.5*	*20*	*10*	*1:1*	*93.31*	*94.83*
17	*3.5*	*10*	*5*	*1:1*	*72.68*	*72.81*
18	*6.0*	*10*	*5*	*1:1*	*54.73*	*54.92*
19	*3.5*	*10*	*10*	*1:1*	*75.42*	*74.27*
20	*6.0*	*10*	*10*	*1:1*	*60.26*	*59.60*
21	*4.5*	*5*	*7.5*	*1:2*	*72.13*	*72.83*
22	*4.5*	*20*	*7.5*	*1:2*	*94.01*	*92.79*
23	*4.5*	*5*	*7.5*	*2:1*	*76.16*	*76.03*
24	*4.5*	*20*	*7.5*	*2:1*	*96.36*	*95.51*
25	*4.5*	*10*	*5*	*1:2*	*80.24*	*78.58*
26	*4.5*	*20*	*5*	*1:1*	*86.77*	*88.82*
27	*4.5*	*10*	*7.5*	*1:1*	*92.61*	*92.18*

Table S4. ANOVA analysis for ranitidine degradation.

Source	Sum of squares	DF	Mean square	*F*-Value	*p*-Value
Model	*4423.74*	*14*	*315.98*	*181.45*	*<0.0001*
X_1	*786.68*	*1*	*786.68*	*451.74*	*<0.0001*
X_2	*852.74*	*1*	*852.74*	*489.67*	*<0.0001*
X_3	*27.61*	*1*	*27.61*	*15.86*	*0.0018*
X_4	*25.18*	*1*	*25.18*	*14.46*	*0.0025*
X_1X_2	*54.22*	*1*	*54.22*	*31.13*	*0.0001*
X_1X_3	*2.65*	*1*	*2.65*	*1.52*	*0.2409*
X_1X_4	*0.94*	*1*	*0.94*	*0.54*	*0.4759*
X_2X_3	*6.41*	*1*	*6.41*	*3.68*	*0.0792*
X_2X_4	*0.068*	*1*	*0.068*	*0.039*	*0.8471*
X_3X_4	*1.31*	*1*	*1.31*	*0.75*	*0.4033*
X_1^2	*1850.61*	*1*	*1850.61*	*1062.68*	*<0.0001*
X_2^2	*263.34*	*1*	*263.34*	*151.22*	*<0.0001*
X_3^2	*215.28*	*1*	*215.28*	*123.62*	*<0.0001*
X_4^2	*102.12*	*1*	*102.12*	*58.64*	*<0.0001*
Residual	*20.90*	*12*	*1.74*		
Lack of Fit	*19.68*	*10*	*1.97*	*3.24*	*0.2590*
Pure Error	*1.22*	*2*	*0.61*		
Cor Total	*4444.64*	*26*			
R-Squared *0.9953*			**Adj R-Squared *0.9898***		

Table S5. Effect of initial solution pH on the reaction rate constant of ranitidine removal.

PH Values	Apparent Reaction Rate Constant			
	Reaction Time from 0 to 3 min		Reaction Time from 3 to 6 min	
	$k1_{obs}$ (min^{-1})	R-Squared	$k2_{obs}$ (min^{-1})	R-Squared
pH=3.5	*0.694*	*0.996*	*0.323*	*0.954*
pH=4.5	*0.572*	*0.999*	*0.268*	*0.991*
pH=6.0	*0.439*	*0.998*	*0.241*	*0.961*
pH=7.0	*0.286*	*0.983*	*0.141*	*0.990*
pH=8.0	*0.189*	*0.963*	*0.083*	*0.994*
pH=9.0	*0.112*	*0951*	*0.048*	*0.994*
pH=10.0	*0.066*	*0.916*	*0.021*	*0.966*

Table S6. Comparison of ranitidine removal efficiency over different technologies.

No.	Methods	Materials	Ranitidine concentration	Ranitidine removal efficiency	Reaction time	Catalysts dosage	k (min^{-1})	Reference
1	Photocatalysis	MoS_2/RGO	10 mg/L	74%	60 min	1 g/L	**0.0208**	11
2	Photocatalysis	MoS_2	10 mg/L	33%	60 min	1 g/L	**0.00599**	11
3	Photocatalysis	RGO	10 mg/L	35%	60 min	1 g/L	**0.00644**	11
4	Photocatalysis	MXene-Ti_3C_2/MoS_2	10 mg/L	88.4%	60 min	1 g/L	**0.03148**	12
5	Photocatalysis	MXene-Ti_3C_2	10 mg/L	18.4%	60 min	1 g/L	**0.0032**	12
6	Photocatalysis	TiO_2	10 mg/L	100%	45 min	0.2 g/L	**0.146**	13
7	Photo-Fenton	TiO_2 + Fe^{2+}/H_2O_2	10 mg/L	100%	22 min	0.2 g/L	**0.23**	13
8	Photocatalysis	TiO_2 Nanofiber	3 mg/L	95%	120 min	--	**0.0080**	14
9	Photocatalysis	Degussa P25 naoparticles	3 mg/L	96%	120 min	--	**0.011**	14
10	Photocatalysis	TiO_2	50 mg/L	60%	5 h	1 g/L	**0.00396**	15
11	UV photolysis	NH_2Cl	5 mg/L	89.4%	5 min	0.051-0.3 g/L	**0.33**	16
12	Heterogeneous Fenton-like catalysis	nZVIPs@Ti_3C_2 nanosheets	10 mg/L	92.3%	6min	0.1 g/L	**0.4311**	This work

Table S7. Adsorption Energy (E_{ads}) of PMS on nZVIPs@Ti_3C_2 nanosheets, the O-O bond length (l_{O-O}) of PMS (HO-OSO_3), and the O-H bond length (l_{O-H}) of PMS (H-$OOSO_3$) in different density functional theory (DFT) models as shown in Fig.6b.

Configuration	E_{ads} (eV)	l_{O-O} (Å)	l_{O-H} (Å)
Free PMS	--	1.326	1.037
Ti_3C_2 nanosheet active-site	-5.43	1.472	0.987
Fe nanoparticle active-site	-4.84	1.474	0.990

References:

[1] Kresse, G.; Furthmüller, J. ***Comput. Mater. Sci.,*** 1996, 6, 15−50.

[2] Kresse, G.; Furthmüller, J. ***Phys. Rev. B.,*** 1996, 54, 11169−11186.

[3] Perdew, J. P.; Burke, K.; Ernzerhof, M. ***Phys. Rev. Lett.,*** 1996, 77, 3865−3868.

[4] Kresse, G.; Joubert, D. ***Phys. Rev. B.,*** 1999, 59, 1758-1775.

[5] Blöchl, P. E. ***Phys. Rev. B.,*** 1994, 50, 17953−17979.

[6] Grimme, S; Antony, J; Ehrlich, S; Krieg, H. ***J. Chem. Phys.,*** 2010, 132, 154104.

[7] Henkelman, G; Uberuaga, B. P; Jonsson, H. ***J. Chem. Phys.,*** 2000, 113, 9901.

[8] Henkelman, G; Jonsson, H. ***J. Chem. Phys.,*** 111 (1999) 7010–7022.

[9] Olsen, R. A; Kroes, G. J; Henkelman, G; Arnaldsson, A; Jonsson, H. ***J. Chem. Phys.***, 121 (2004) 9776–9792.

[10] Heyden, A; Bell, A. T; Keil, F. J. ***J. Chem. Phys.,*** 123 (2005) 224101.

[11] Zou, X; Zhang, J. X; Zhao, X. S; Zhang, Z. H. ***Chem. Eng. J.***, 383 (2020) 123084.

[12] Zou, X; Zhang, Z. H; Zhang, J. X; Lv, W; Qiu, L; Zhang, Z. H. ***J. Hazard. Mater.***, 413 (2021) 125424.

[13] Jelena. R; Carla, S; Mira. P; Damià, B; Sixto, M. ***Chemospere.***, 79 (2010) 368-376.

[14] Choi, K. J; Hong, S. W. ***Res.Chem. Intermed.,*** 38(2012)1161–1169.

[15] Addamo, M; Augugliaro, V; Dipaola, A; García-lópez, E; Loddo, V; MarcÌ, G; Palmisano, L. ***J Appl. Electrochem.***, 35 (2005) 765-774.

[16] Wu, Y. T; Zhu, S. M; Wang, J; Bu, L. J; Deng, J; Zhou, S. Q. ***Chem. Eng. J.***, 404 (2021) 126557.